PERGAMON

International Journal of Heat and Mass Transfer 42 (1999) 709–722

International Journal of HEAT and MASS TRANSFER

Transition and multiplicity of flows in natural convection in a narrow horizontal cylindrical annulus: $Pr = 0.4$

Joo-Sik Yoo*

Department of Mechanical Engineering Education, Andong National University, 388 Songchun-dong, Andong, Kyungpuk, 760-749 Korea

Received 2 March 1998, in final form 4 June 1998

Abstract

Natural convection in a narrow horizontal concentric annulus is numerically investigated for a fluid of $Pr = 0.4$. The combined effect of thermal and hydrodynamic instability at $Pr = 0.4$ yields complex multicellular flow patterns and interesting transition phenomena. After the onset of instability of the conduction regime, four branches of solutions and five kinds of multiple solutions characterized by the temporal behaviour and spatial structure of flows are found. As Gr increases, the transition of flow structure shows a gradual increase in the number of cells. When Gr is further increased, the flow in the vertical section of the annulus reverts to a nearly monocellular structure. A transition phenomenon from oscillatory to steady flow is found with an increase in Gr.

Nomenclature

D_i diameter of inner cylinder
Gr Grashof number based on the gap width, $\alpha g(T_i - T_o)L^3/v^2$
g acceleration of gravity
J Jacobian
L gap width of the annulus, $R_o - R_i$
$N_{(\text{cells on top})}$ number of cells separated by the streamline of $\psi = 0$ on the top of the annulus
Nu_{cond} Nusselt number of pure conduction state
Nu_i, Nu_o local Nusselt numbers at the inner and outer cylinders, respectively
$\overline{Nu}_i$, $\overline{Nu}_o$ mean Nusselt numbers at the inner and outer cylinders, respectively
$\overline{Nu}(t)$ overall Nusselt number, $(\overline{Nu}_i + \overline{Nu}_o)/2$
$\overline{Nu}_{time}$ time-averaged overall Nusselt number
P period of oscillation
Pr Prandtl number, v/χ
Ra Rayleigh number, $PrGr$
R_i. R_o radii of the inner and outer cylinders, respectively
r dimensionless radial coordinate
r_i, r_o dimensionless radii of the inner and outer cylinders, respectively
r_c radial coordinate of the center of annular gap, $(r_i + r_o)/2$
t dimensionless time
T_i, T_o temperatures at the inner and outer cylinders, respectively
u, v dimensionless velocity components in the radial and angular directions, respectively
$u(t)$ instantaneous radial velocity at $(r_c, \pi/2)$, $u(r_c, \pi/2, t)$.

Greek symbols
α coefficient of thermal expansion
η stretched coordinate in the radial direction
θ dimensionless temperature
χ thermal diffusivity
v kinematic viscosity
ρ_0 mean density
ϕ angular coordinate
ψ dimensionless streamfunction
ω dimensionless vorticity

1. Introduction

Natural convection in a horizontal cylindrical annulus has received much attention because of the theoretical interest and its wide engineering applications such as

* Corresponding author. E-mail: jsyoo@anu.andong.ac.kr

0017–9310/98 $19.00
PII: S0017–9310(98)00197–5

thermal energy storage systems, cooling of electronic components and transmission cables. Comprehensive reviews on this problem were presented by Gebhart et al. [1] and Yoo [2, 3].

The basic flow field for low value of Gr forms two symmetric kidney-shaped (or crescent-shaped) eddies in which fluid rises near the inner hotter cylinder and sinks near the outer colder one. As Gr increases, however, several kinds of convective flows which are dependent on Pr and the aspect ratio can be developed. Powe et al. [4, 5] and Rao et al. [6] investigated flow patterns of air, and found three flow regimes depending on diameter ratio (D_i/L): a two-dimensional oscillatory flow for $D_i/L < 2.8$, a three-dimensional spiral flow for $2.8 < D_i/L < 8.5$, and a two-dimensional multicellular flow for $D_i/L > 8.5$. Some other authors considered low-Prandtl-number fluids, and showed several kinds of multicellular flows [7–9].

To date, many authors have studied natural convection in wide-gap annuli. However, relatively few studies have been made for narrow annuli [10, 11]. On the other hand, the natural convection problems in a vertical slot [12–15] and in a tall vertical annulus [16, 17] have been studied extensively.

Recently, the present author considered the natural convection problem in a narrow horizontal annulus with $D_i/L = 12$, and investigated the effect of Prandtl number on the stability of conduction regime [3]. It was observed that the stability of the conduction regime of natural convection can be classified into two regimes: (i) at $Pr \leqslant 0.2$, the instability sets in as steady or oscillatory flows consisting of multiple like-rotating cells in the vertical section of the annulus; (ii) at $Pr \geqslant 0.3$, the instability first sets in at the top portion of the annulus. The conduction-dominated regime of natural convection for low value of Gr forms a crescent-shaped eddy in a half annulus. After the onset of instability of conduction regime, very complex multicellular convection is developed, and the flow patterns have been observed to be strongly dependent on the Prandtl number. The results for $Pr \leqslant 0.3$ were presented previously by this author [3]. And in this study, the convective motion of a fluid with $Pr = 0.4$ will be investigated.

In a narrow horizontal annulus with a heated inner cylinder, there are two instability mechanisms present in flow. One is the Rayleigh–Bénard thermal instability [18] which operates on the top part of the thermally unstable region, and the other is the shear driven hydrodynamic instability in the near vertical section. The hydrodynamic instability has been observed at low values of Pr [10, 11], and the thermal instability at high Pr [19]. At the intermediate value of Prandtl number, the two instability mechanisms can be coexistent. As a result, this study observed very complex multicellular flow patterns and interesting transition phenomena for $Pr = 0.4$. The main features are discussed here.

The flow field after the onset of instability of conduction regime consists of square-shaped closed cells on the top of annulus and one or more like-rotating cells in the vertical section. As Gr increases starting from the value of conduction regime, the transition of flow structure shows gradual increase in the number of cells. At high Gr, however, the number of cells decreases with increase of Gr, that is, a transition from a multicellular flow to a flow with fewer cells occurs. The hysteresis phenomenon is also observed between the solution branches characterized by the number of cells. This study found five kinds of multiple solutions characterized by the temporal behavior and spatial structure of flows: (i) dual steady flows; (ii) one steady and one oscillatory flows; (iii) one steady and two oscillatory flows; (iv) dual oscillatory flows; (v) triple oscillatory flows. At small Gr, the like-rotating cells created in the upper part of the annulus drift downward and disappear in the lower region of the annulus. At relatively high Gr, however, the cells do not drift into the lower half of the annulus, and the phenomena of coalescence and separation of two like-rotating cells occur in the lower or upper region of the annulus. The temporal behavior of the flow field was observed to be closely related to the motion of cells. As a result, a transition phenomenon of 'steady → oscillatory → steady → oscillatory flow' was found, with increase of Gr.

A notable one for $Pr = 0.4$ is the diverse multiple solutions which appear after the instability of conduction state. And it can be compared with the multiple steady solutions observed in the other hydrodynamic problems (Taylor problem, Dean problem, natural convection, etc.) [20–24]. In a narrow horizontal annulus with a heated cylinder, the combined effect of thermal and hydrodynamic instability can yield diverse multiple flow patterns compared with the cases of a vertical slot [12–15], a tall vertical annulus [16, 17], and other hydrodynamic problems [20–24].

2. Analysis

The fluid is contained between two infinite horizontal concentric circular cylinders, which are held at different uniform temperatures of T_i and T_o ($T_i > T_o$). The thermophysical properties of fluid, except density, are assumed constant. And the Boussinesq approximation is employed such that the variation of density with temperature can be neglected except for the buoyancy force terms. The viscous dissipation in the energy equation is also neglected. We consider a two-dimensional problem, and use the cylindrical coordinates (r, ϕ), the angular coordinate ϕ being measured counter-clockwise from the upward vertical through the center of the cylinders (Fig. 1). The equations governing conservation of mass, momentum, and energy are put into non-dimensional form by taking the characteristic length, time, velocity,

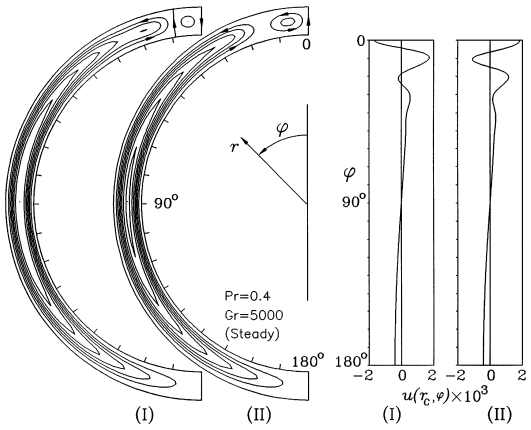

Fig. 1. Steady-state streamlines and radial velocity distributions at the centerline of annular gap, $u(r_c, \phi)$, at $Gr = 5000$: the solutions with a counter-rotating cell (I) and a like-rotating cell (II) on the top of the annulus.

pressure, and temperature as L, L^2/ν, $V = \alpha g(T_i - T_o)L^2/\nu$, $\rho_0 V^2$, and $(T_i - T_o)$, respectively. We let $Pr = \nu/\chi$ and $Gr = \alpha g(T_i - T_o)L^3/\nu^2$ denote the Prandtl and Grashof numbers, respectively. The dimensionless equations governing the two-dimensional convection in terms of vorticity (ω) and streamfunction (ψ) are written as follows:

$$\frac{\partial \omega}{\partial t} = Gr\, J(\psi, \omega) + \nabla^2 \omega - \left[\sin(\phi)\frac{\partial \theta}{\partial r} + \cos(\phi)\frac{\partial \theta}{r\,\partial \phi} \right] \quad (1)$$

$$\omega = -\nabla^2 \psi \quad (2)$$

$$\frac{\partial \theta}{\partial t} = Gr\, J(\psi, \theta) + \frac{1}{Pr}\nabla^2 \theta \quad (3)$$

where the vorticity ω, streamfunction ψ, Jacobian $J(f, g)$, and Laplacian ∇^2 are

$$\omega = \frac{\partial}{r\,\partial r}(rv) - \frac{\partial}{r\,\partial \phi}(u), \quad u = \frac{\partial \psi}{r\,\partial \phi}, \quad v = -\frac{\partial \psi}{\partial r}$$

$$J(f, g) = \frac{1}{r}\left(\frac{\partial f}{\partial r}\frac{\partial g}{\partial \phi} - \frac{\partial f}{\partial \phi}\frac{\partial g}{\partial r} \right)$$

$$\nabla^2 = \frac{\partial}{r\,\partial r}\left(r\frac{\partial}{\partial r} \right) + \frac{\partial^2}{r^2\,\partial \phi^2} \quad (4)$$

The boundary conditions on the two walls are

$$\psi = \frac{\partial \psi}{\partial r} = 0, \quad \omega = -\frac{\partial^2 \psi}{\partial r^2}, \quad \theta = 1 \quad \text{at} \quad r = r_i \quad (5)$$

$$\psi = \frac{\partial \psi}{\partial r} = 0, \quad \omega = -\frac{\partial^2 \psi}{\partial r^2}, \quad \theta = 0 \quad \text{at} \quad r = r_o \quad (6)$$

We impose the following symmetric conditions

$$\psi = \omega = \frac{\partial^2 \psi}{\partial \phi^2} = \frac{\partial \theta}{\partial \phi} = 0 \quad \text{at} \quad \phi = 0, \pi \quad (7)$$

since we suppose the flow to be symmetric with respect to the vertical plane through the center of cylinders.

The dimensionless heat transfer rate of pure conduction in the absence of fluid motion is

$$Nu_{cond} = \frac{1}{\ln(r_o/r_i)} \quad (8)$$

The local Nusselt number is defined as the actual heat flux divided by Nu_{cond}

$$Nu_i(\phi) = -\left(r\frac{\partial \theta}{\partial r} \right) / Nu_{cond} \quad \text{at} \quad r = r_i \quad (9)$$

$$Nu_o(\phi) = -\left(r\frac{\partial \theta}{\partial r} \right) / Nu_{cond} \quad \text{at} \quad r = r_o \quad (10)$$

And the mean Nusselt numbers, $\overline{Nu_i}$ and $\overline{Nu_o}$, are given by

$$\overline{Nu_i} = \frac{1}{\pi}\int_0^\pi Nu_i(\phi)\, d\phi \quad (11)$$

$$\overline{Nu_o} = \frac{1}{\pi}\int_0^\pi Nu_o(\phi)\, d\phi \quad (12)$$

Equations (1)–(7) are numerically solved by the same finite difference method used in [3]. Equations (1) and (3) are cast into finite difference form using the leap-frog method [25] of Dufort–Frankel for the diffusion and time derivative terms, and central differencing for the Jacobian. The Poisson equation for the streamfunction is discretized by use of five-point formula, and the discretized equation is solved by the direct method of Buzbee et al. [26] which uses cyclic even–odd reduction method. In the azimuthal direction, a uniform grid is employed, and in the radial direction, the following coordinate stretching is utilized:

$$r = r_i + \frac{1}{2}\left[1 + \frac{\tanh\{C(2\eta - 1)\}}{\tanh(C)} \right] \quad \text{with} \quad C = 1.5, \quad 0 \leqslant \eta \leqslant 1 \quad (13)$$

This study uses the $(r \times \phi)$ meshes of (17×257). The time step Δt is taken in the range of $10^{-5} \leqslant \Delta t \leqslant 10^{-3}$.

To investigate the oscillatory flow, we record the time variation of the integrated value of local Nusselt number, $\overline{Nu}(t)$, and the following radial velocity at the center of annular gap during the computational period:

$$u(t) = u(r_c, \pi/2, t) \quad \text{where} \quad r_c = (r_i + r_o)/2 \quad (14)$$

The point of $(r_c, \pi/2)$ is chosen as a measuring point, since hydrodynamic instability occurs in the vertical section of annulus.

3. Results and discussion

Computations were performed for an annulus of $D_i/L = 12$ in the range of $Gr \leqslant 8 \times 10^4$. The parametric study for Gr was made with the increments of $\Delta Gr = 500$, 1000, or 2000 to find diverse transition phenomena of flow patterns.

When $Pr = 0.4$, the conduction-dominated flow is maintained up to $Gr = 4500$, but the flow becomes unstable with increase of Gr, and finally a new flow pattern with a counter-rotating cell on the top of annulus is established at $Gr = 5000$. The steady-state streamlines with a counter-rotating cell and the distribution of radial velocities are presented in Fig. 1(I). A notable one for $Pr = 0.4$ is that if we use the solution of the higher Ra with two (or four) cells on the top (Fig. 2(a), (d)) as the initial condition, a new flow with a small like-rotating cell on the top (Fig. 1(II)) is obtained at $Gr = 5000$. For both cases, however, the streamlines and the velocity profiles are nearly identical to those of the conduction regime except the thermally unstable region of the top of the annulus ($0 < \phi < 40^\circ$). The values of $Gr = 5000$ and $Pr = 0.4$ give $Ra = 2000$, which can be compared with the critical Rayleigh number of $Ra_c = 1708$ in the Rayleigh–Bénard convection [18].

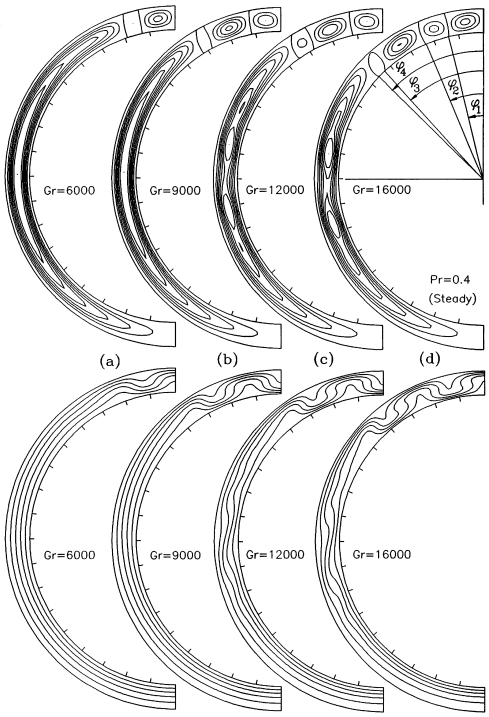

Fig. 2. Steady-state streamlines and isotherms for the flows having two (a), three (b, c), and four (d) cells on the top of the annulus: (a) $Gr = 6000$; (b) $Gr = 9000$; (c) $Gr = 1.2 \times 10^4$; (d) $Gr = 1.6 \times 10^4$.

After the onset of instability of the conduction regime ($Gr \geqslant 5000$), diverse multicellular flow patterns and bifurcation phenomena are observed. The flow has one (Fig. 1), two (Fig. 2(a)), three (Fig. 2(b), (c)), or four (Fig. 2(d)) cells on the top of the annulus, and one or more like-rotating cells in the vertical section. We classify the flow patterns by the number of the cells on the top. The branches of solutions found are presented in Fig. 3. The solutions in Fig. 3 are characterized by the number of cells separated by the streamline of $\psi = 0$ on the top of the annulus. The smallest Grashof numbers for the solution branches of $N_{(\text{cells on top})} = 1$, 2, 3, and 4 are $Gr = 5000$, 6000, 9000, and 1.6×10^4, respectively, and it is notable that all the flows at those values of Gr are steady. From Fig. 3, we can see various types of multiple solutions: (i) dual steady solutions, (ii) one steady + one oscillatory, (iii) one steady + two oscillatory, (iv) dual oscillatory, (v) triple oscillatory solutions. A hysteresis phenomenon is also observed between the branches of $N_{(\text{cells on top})} = 1$ and 3.

At first we present the results for the solution branches of $N_{(\text{cells on top})} = 1$ and 3. When Gr is increased starting from the conduction-dominated flow of low Grashof number having a crescent-shaped eddy, the flow with a counter-rotating cell or three cells on the top is obtained at $Gr \geqslant 5000$ (Fig. 3). The characteristics of flows for these branches can be summarized as follows, and will be explained later:

(1) $5000 \leqslant Gr \leqslant 7000$: Steady convection with a counter-rotating cell on the top (Fig. 1(I)) is maintained.
(2) $8000 \leqslant Gr \leqslant 9000$: Oscillatory convection with a counter-rotating cell, in which a weak like-rotating cell appears and disappears periodically near $\phi = 25^\circ$, occurs. At $Gr = 9000$, a steady flow with three cells on the top (Fig. 2(b)) is also obtained, if we use the solution of the higher Gr in the branch of $N_{(\text{cells on top})} = 3$ as an initial condition (Fig. 3).
(3) $10^4 \leqslant Gr \leqslant 1.1 \times 10^4$: Oscillatory convection (Fig. 4) with three cells on the top part and two or more like-rotating cells in the vertical section of the annulus occurs. The like-rotating cells created in the upper part of the annulus drift downward as time goes on (Fig. 5).
(4) $Gr = 1.2 \times 10^4$: A steady convection with three cells on the top and four like-rotating cells in the vertical section of the annulus (Fig. 3(c)) is obtained.
(5) $1.3 \times 10^4 \leqslant Gr \leqslant 4 \times 10^4$: Oscillatory convection with three cells on the top and two or more like-rotating cells in the vertical section of the annulus occurs. The cells in the upper part of the chain of like-rotating cells ($\phi < 90^\circ$) do not drift into the lower half of the annulus ($\phi > 90^\circ$). Instead, the phenomena of coalescence and separation of two like-rotating cells

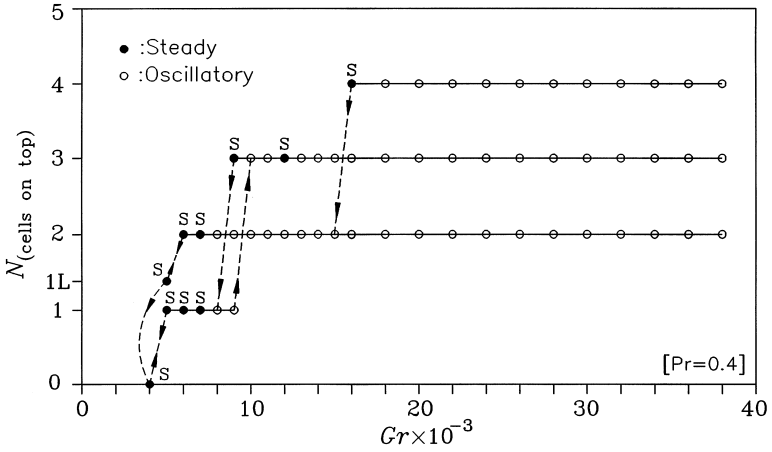

Fig. 3. Diagram showing the branches of solutions: $N_{(\text{cells on top})} = 1, 2, 3$, and 4 represent the numbers of cells separated by the streamline of $\psi = 0$ on the top of the annulus. $N_{(\text{cells on top})} = 1\text{L}$ represents the solution having one like-rotating cell on the top (Fig. 1(II)). (●) steady solutions; (○) unsteady oscillatory solutions.

occur in the lower or upper region of the annulus (Figs 6 and 7).

The time evolutions of $u(t)$ and $\overline{Nu}(t)$ for several Grashof numbers ($Gr = 1.1\times10^4$, 1.3×10^4, 2×10^4, 2.8×10^4, and 3.4×10^4) in the solution branch of $N_{(\text{cells on top})} = 3$ are shown in Fig. 4. In this branch, oscillatory convection occurs at $Gr \geqslant 10^4$. At the initial stage of oscillatory convection ($10^4 \leqslant Gr \leqslant 1.1\times10^4$), the unsteady motion is periodic in time, and occurs relatively slowly (Fig. 4(a)). However, the fluctuations at $Gr = 1.3\times10^4$ show relatively fast oscillation (Fig. 4(b)). And the fluctuation undergoes more complicated oscillations (Fig. 4(c), (d)) with increase of Gr, and afterwards a new time-periodic motion is developed again (Fig. 4(e)). This behavior is observed to be closely related to the transition phenomena of the motion of cells.

The periodic motion of cells at $Gr = 1.1\times10^4$ is shown in Fig. 5. The figure shows three cells on the top part of the annulus, and it can be clearly seen that the like-rotating cells in the vertical section drift downward as time goes on. A cell drifts below the central line of the annulus ($\phi = 90^\circ$), and coalescence of cells occurs near $\phi = 105^\circ$. During this period, a new cell is created in the space of the top portion of the chain of like-rotating cells. When $Gr = 1.3\times10^4$ (Fig. 6), however, the cells in the upper half of the annulus ($\phi < 90^\circ$) do not drift into the lower half ($\phi > 90^\circ$). Figure 6 shows coalescence and separation of cells in the upper half of the annulus, and it can be seen that the cell near $\phi = 80^\circ$ does not drift below the central line of the annulus ($\phi = 90^\circ$).

The above-mentioned results for $Gr = 1.1\times10^4$ and 1.3×10^4 show completely different characteristics for the motion of like-rotating cells in the vertical section of the annulus. We can see that there are two kinds of driving force, one makes the cells drift downward, but the other inhibits. At the intermediate value of $Gr = 1.2\times10^4$, a balance is maintained between the two kinds of force, and a steady-state flow is established. The steady-state streamlines of $Gr = 1.2\times10^4$ in Fig. 2 show four like-rotating cells in the vertical section, which are nearly symmetric about the central line of the annulus ($\phi = 90^\circ$). At the higher Grashof number of $Gr = 1.3\times10^4$, oscillatory convection is developed again (Fig. 4(b)).

As Gr is increased, the region occupied by the three closed cells on the top part of the annulus becomes wider and the oscillatory flow shows coalescence and separation of cells clearly in the lower part of the annulus at high Gr. The instantaneous streamlines at $Gr = 3.4\times10^4$ are presented in Fig. 7. The figure shows the phenomena clearly in the region of $90^\circ < \phi < 140^\circ$. The oscillatory motion of the upper portion of the chain of like-rotating cells, however, shows that the strongest cell near $\phi = 80^\circ$ oscillates periodically in the azimuthal direction with a small amplitude of displacement. The two periodic flows of $Gr = 1.3\times10^4$ (Fig. 6) and $Gr = 3.4\times10^4$ (Fig. 7) show a transition of flow patterns, and we can see that a new time-periodic flow occurs after experiencing a variation of flow structure with increase of Gr.

In the branch of $N_{(\text{cells on top})} = 2$, the flow field has two square-shaped cells on the top of the annulus (Fig. 2(a)). The flow pattern exists at $Gr \geqslant 6000$ (Fig. 3). The flow is steady for $6000 \leqslant Gr \leqslant 7000$, but oscillatory convection is developed at $Gr \geqslant 8000$ (Fig. 8). The observed phenomena for this branch are as follows:

(1) $Gr = 8000$: The oscillation is weak, and the motion of cells is not apparently visible.
(2) $9000 \leqslant Gr \leqslant 1.8\times10^4$: During the oscillation period,

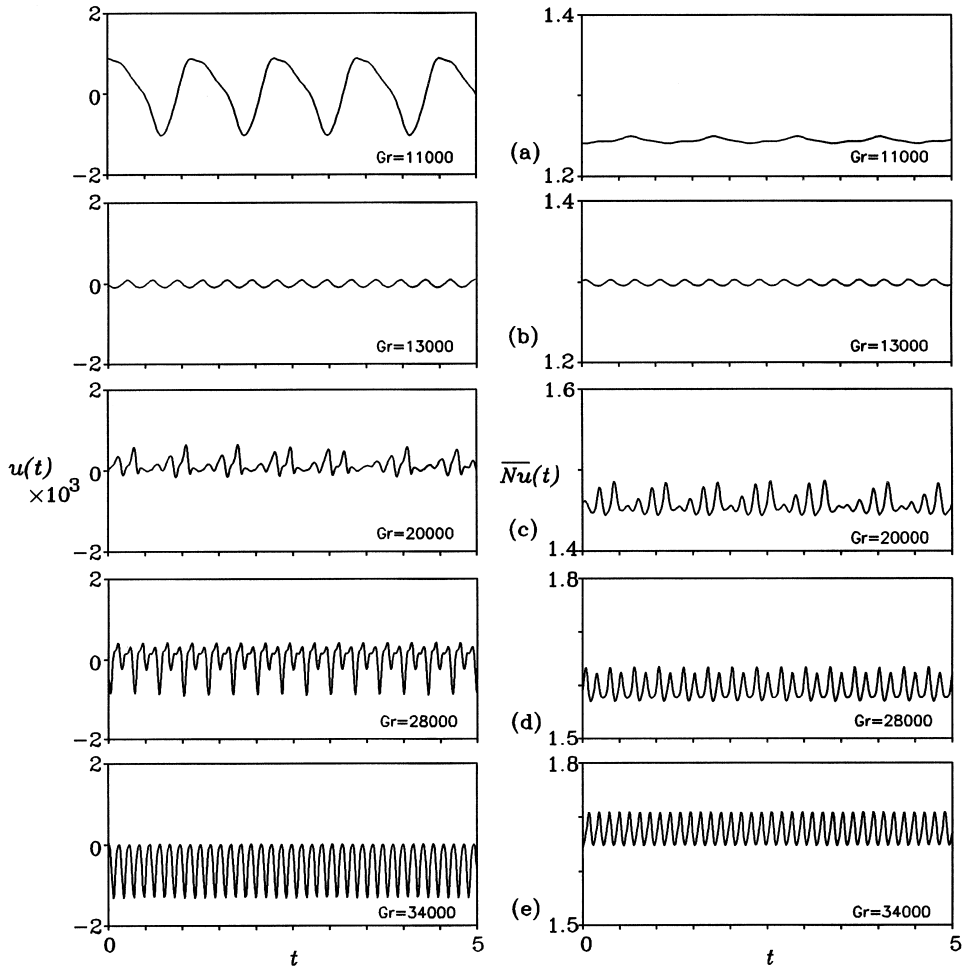

Fig. 4. Time evolutions of $u(t)$ and $\overline{Nu}(t)$ for several Grashof numbers in the solution branch of $N_{(\text{cells on top})} = 3$: (a) $Gr = 1.1 \times 10^4$; (b) $Gr = 1.3 \times 10^4$; (c) $Gr = 2 \times 10^4$; (d) $Gr = 2.8 \times 10^4$; (e) $Gr = 3.4 \times 10^4$.

a new cell is created in the top portion of the chain of like-rotating cells in the vertical section of the annulus. As time goes on, it drifts downward, and coalescence of cells occurs near $\phi = 90^\circ$, 100° and 105°, for $9000 \leqslant Gr \leqslant 10^4$, 1.2×10^4 and $1.4 \times 10^4 \leqslant Gr \leqslant 1.8 \times 10^4$, respectively, i.e., the location moves slightly downward with increase of Gr.

(3) At $Gr \geqslant 2 \times 10^4$, the cells in the upper half of the annulus ($\phi < 90^\circ$) do not drift into the lower half ($\phi > 90^\circ$), with the result that
   (i) $2 \times 10^4 \leqslant Gr \leqslant 3.6 \times 10^4$: When $Gr = 2 \times 10^4$, a strong cell is formed near $\phi = 90^\circ$, and the cell oscillates periodically in the azimuthal direction with a small amplitude of displacement ($\Delta\phi < 5^\circ$). The upper part of the chain of like-rotating cells ($\phi < 90^\circ$) displays coalescence and separation of cells. The cell located near $\phi = 90^\circ$ for $Gr = 2 \times 10^4$ is slightly shifted downward with an increase in Gr: the center of the cell locates near $95^\circ < \phi < 100^\circ$ at $Gr = 3.6 \times 10^4$.
   (ii) $3.8 \times 10^4 \leqslant Gr \leqslant 4 \times 10^4$: Coalescence and separation of cells occur near $\phi = 110^\circ$. During the oscillation period, a weak small like-rotating eddy appears and disappears intermittently near $\phi = 90^\circ$.

The fluctuations of $u(t)$ and $\overline{Nu}(t)$ for the flows with $N_{(\text{cells on top})} = 2$ (Fig. 8) also show the establishment of a new periodic flow (Fig. 8(d)) after experiencing the more complicated oscillations (Fig. 8(b), (c)) with increase of Gr. The further increase of Gr creates intermittent noise, and leads to non-periodic motion again (Fig. 8(e)).

As an example of the motion of cells in the solution branch of $N_{(\text{cells on top})} = 2$, the instantaneous streamlines

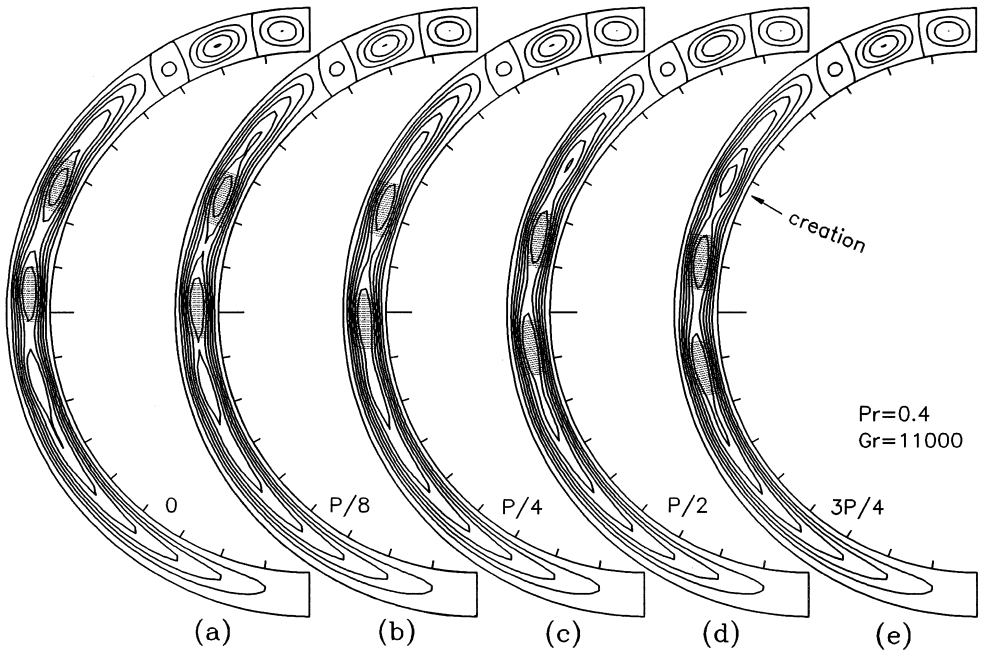

Fig. 5. Time sequence of streamfunction field over one period of oscillation at $Gr = 1.1 \times 10^4$, in the solution branch of $N_{(\text{cells on top})} = 3$; (a) at $t = t_1$ at which $u(t)$ takes its minimum value; (b) at $t = t_1 + P/8$; (c) at $t = t_1 + P/4$; (d) at $t = t_1 + P/2$; (e) at $t = t_1 + 3P/4$. Two structures are shaded with dots so that their motions can be followed.

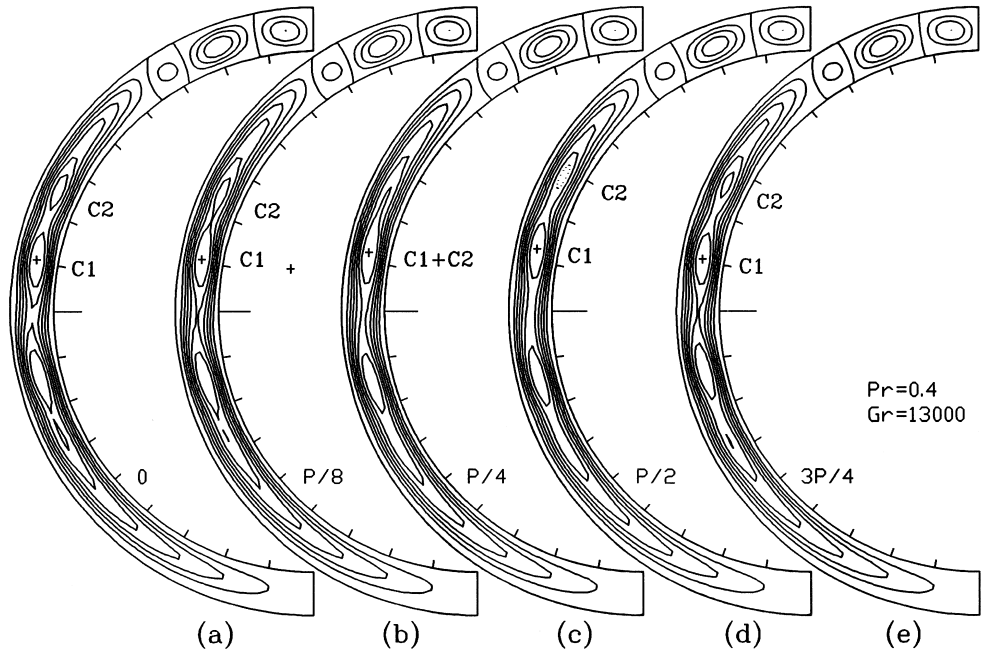

Fig. 6. Time sequence of streamfunction field over one period of oscillation at $Gr = 1.3 \times 10^4$, in the solution branch of $N_{(\text{cells on top})} = 3$: (a) at $t = t_1$ at which $u(t)$ takes its minimum value; (b) at $t = t_1 + P/8$; (c) at $t = t_1 + P/4$; (d) at $t = t_1 + P/2$; (e) at $t = t_1 + 3P/4$.

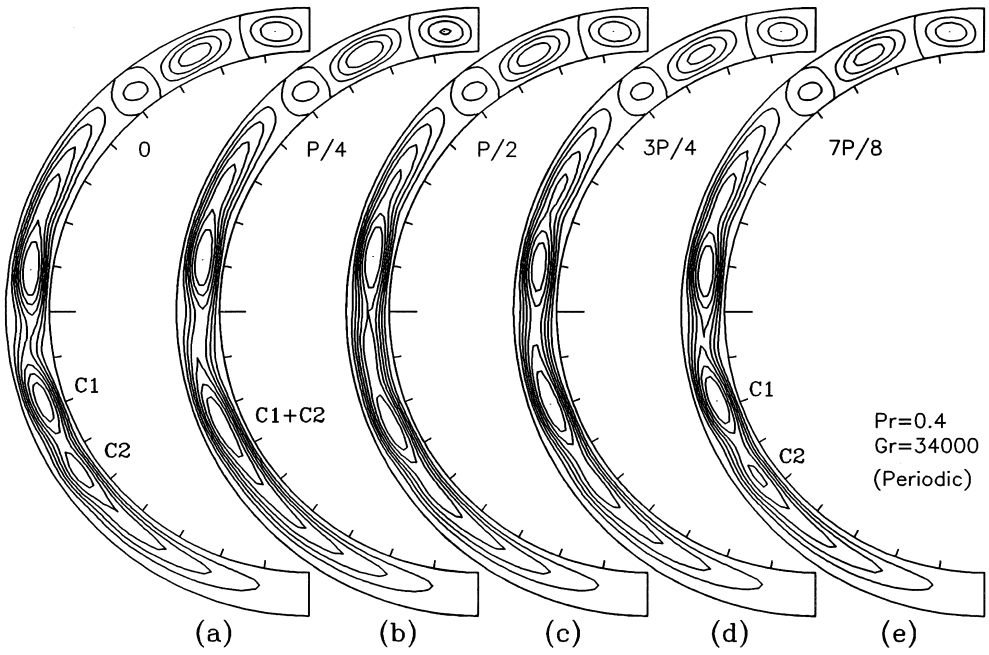

Fig. 7. Time sequence of streamfunction field over one period of oscillation at $Gr = 3.4 \times 10^4$, in the solution branch of $N_{(\text{cells on top})} = 3$: (a) at $t = t_1$ at which $u(t)$ takes its minimum value; (b) at $t = t_1 + P/4$; (c) at $t = t_1 + P/2$; (d) at $t = t_1 + 3P/4$; (e) at $t = t_1 + 7P/8$.

at $Gr = 3.4 \times 10^4$ are presented in Fig. 9 to compare with those of $N_{(\text{cells on top})} = 3$ in Fig. 7. The figure shows two cells on the top and three or more like-rotating cells in the vertical section of the annulus. Unlike the case with $N_{(\text{cells on top})} = 3$ in Fig. 7, the cells below the central line of the annulus ($\phi > 90^\circ$) oscillate periodically in the azimuthal direction, and coalescence and separation of cells is clearly visible in the upper part of the chain of like-rotating cells ($\phi < 90^\circ$).

The flow having four cells on the top (Fig. 2(d)) exists at $Gr \geqslant 1.6 \times 10^4$ (Fig. 3). The phenomena observed for the solution branch of $N_{(\text{cells on top})} = 4$ up to $Gr = 4 \times 10^4$ are as follows:

(1) When $Gr = 1.6 \times 10^4$, a steady-state flow with clearly visible two like-rotating cells in the vertical section of the annulus is established (Fig. 2(d)). The mechanism for steady state is similar to that of $Gr = 1.2 \times 10^4$ with $N_{(\text{cells on top})} = 3$ showing a balance of driving forces (Fig. 2(c), Figs 5–6), one makes the cells drift downward, but the other inhibits.

(2) At $1.8 \times 10^4 \leqslant Gr \leqslant 4 \times 10^4$, however, oscillatory convection is developed (Fig. 10). The oscillatory flow also has two like-rotating cells in the vertical section which are similar to those in Fig. 2(d). During the oscillation period, the cells in each region of $\phi < 90^\circ$ and $\phi > 90^\circ$ do not cross over the central line of the annulus ($\phi = 90^\circ$). In $\phi < 90^\circ$, the phenomena of coalescence and separation of cells are not clearly visible, but the center of the strong cell located near $80^\circ < \phi < 85^\circ$ oscillates in the azimuthal direction with a small amplitude of displacement ($\Delta\phi < 5^\circ$). In the lower half of the annulus ($\phi > 90^\circ$), coalescence and separation of like-rotating cells is visible. The point at which coalescence of cells occurs is near $110^\circ < \phi < 120^\circ$ for $1.8 \times 10^4 \leqslant Gr \leqslant 4 \times 10^4$. As Gr is increased, the point of the center of the strong cell in $\phi < 90^\circ$ and coalescence of cells occurs in $\phi > 90^\circ$ move slightly downward.

The oscillatory convections in the solution branch of $N_{(\text{cells on top})} = 4$ are nearly periodic in time up to $Gr = 4 \times 10^4$. The fluctuations of $u(t)$ and $\overline{Nu}(t)$ at $Gr = 2 \times 10^4$ and 3.4×10^4 are presented in Fig. 10 to compare the triple oscillatory solutions of $N_{(\text{cells on top})} = 2$, 3, 4 (Fig. 3). The fluctuations in the branches of $N_{(\text{cells on top})} = 2$ and 3 are shown in Fig. 8 and Fig. 4, respectively. At $Gr = 2 \times 10^4$, the flows having two (Fig. 8(c)) and three (Fig. 4(c)) cells on the top display irregular oscillations, but periodic motion is developed for the flow with four cells (Fig. 10(a)). In the case of $Gr = 3.4 \times 10^4$, all the flows show periodic fluctuations (Figs 4(e), 8(d) and 10(b)). From the figures of $\overline{Nu}(t)$, we can see that the mean values of $\overline{Nu}(t)$, $\overline{Nu}_{\text{mean}}$, for the triple solutions have the following order of magnitude:

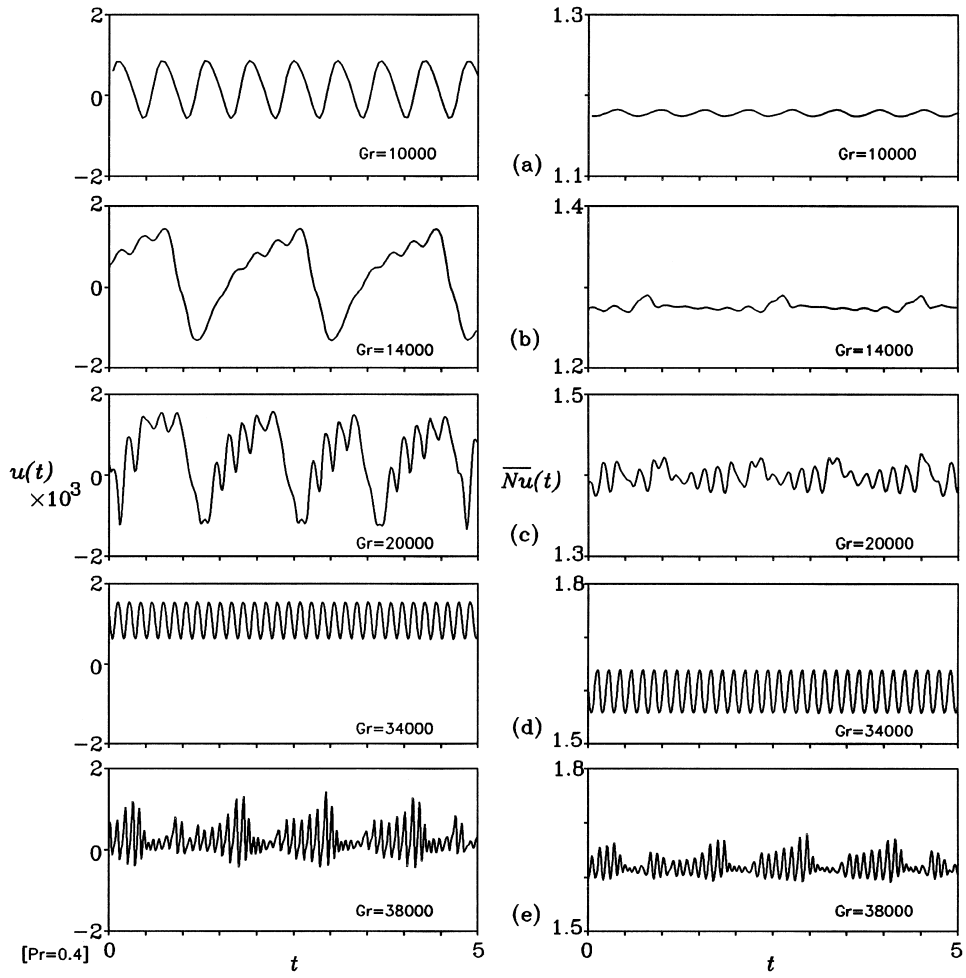

Fig. 8. Time evolutions of $u(t)$ and $\overline{Nu}(t)$ for several Grashof numbers in the solution branch of $N_{(\text{cells on top})} = 2$: (a) $Gr = 10^4$; (b) $Gr = 1.4 \times 10^4$; (c) $Gr = 2 \times 10^4$; (d) $Gr = 3.4 \times 10^4$; (e) $Gr = 3.8 \times 10^4$.

$\overline{Nu}_{\text{mean}}$ (4) > $\overline{Nu}_{\text{mean}}$ (3) > $\overline{Nu}_{\text{mean}}$ (2), where the numbers in the parentheses represent $N_{(\text{cells on top})}$.

An example of the transient development of cells in the branch of $N_{(\text{cells on top})} = 4$ after impulsive heating of the cylinder is shown in Fig. 11 with $Gr = 1.6 \times 10^4$. The initial conditions are $\vec{u} = \theta = 0$, and the inner cylinder is suddenly heated to $\theta = 1$. After a second, a pseudo-conduction state with a crescent-shaped cell is established (Fig. 11(a)). And afterwards instability occurs in the vertical section of the annulus, creating like-rotating cells (Fig. 11(b)). The instability propagates along the circumference of the annulus, and new cells are successively created (Fig. 11(c), (d)). As time goes on, all the cells except the cells on the top of the annulus tend to drift downward. During this course, two new counter-rotating cells are created at the boundaries of a strong cell on the top, and grow in size (Fig. 11(e), (f)). After the creation of the four closed cells, the region occupied by the cells on the top of the thermally unstable region becomes wider; and the strength of the cell near $\phi = 0$ in which the vertical temperature gradient between two cylinders is the greatest is also increased (Fig. 11(g), (h)).

The effect of flow pattern on the distribution of local Nusselt numbers at the walls is shown in Fig. 12 with $Gr = 3.4 \times 10^4$ which has triple oscillatory solutions. The multicellular flow makes the distribution very complex. At the boundaries of cells on the top of the annulus, $Nu(\phi)$ has relative minimum or maximum values, and accordingly, the different number of cells yields large local variations of Nusselt numbers, especially on the top part of the annulus.

Figure 13 presents time-averaged overall Nusselt number ($\overline{Nu}_{\text{time}}$) as functions of Gr. The figures shows a relatively steep increase (or decrease) in the overall Nusselt

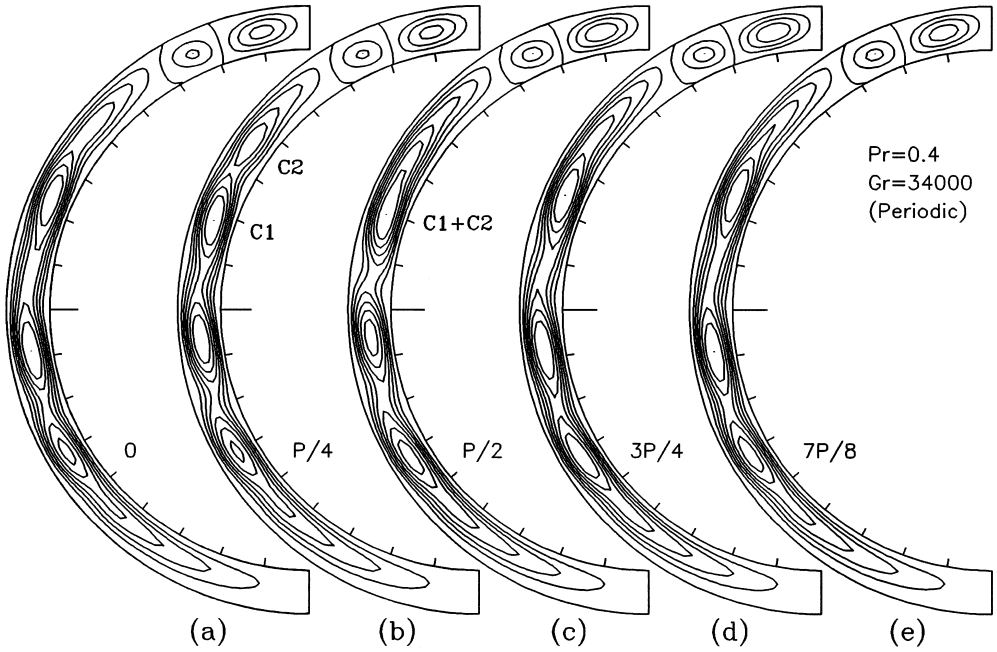

Fig. 9. Time sequence of streamfunction field over one period of oscillation at $Gr = 3.4 \times 10^4$, in the solution branch of $N_{(\text{cells on top})} = 2$: (a) at $t = t_1$ at which $u(t)$ takes its minimum value; (b) at $t = t_1 + P/4$; (c) at $t = t_1 + P/2$; (d) at $t = t_1 + 3P/4$; (e) at $t = t_1 + 7P/8$.

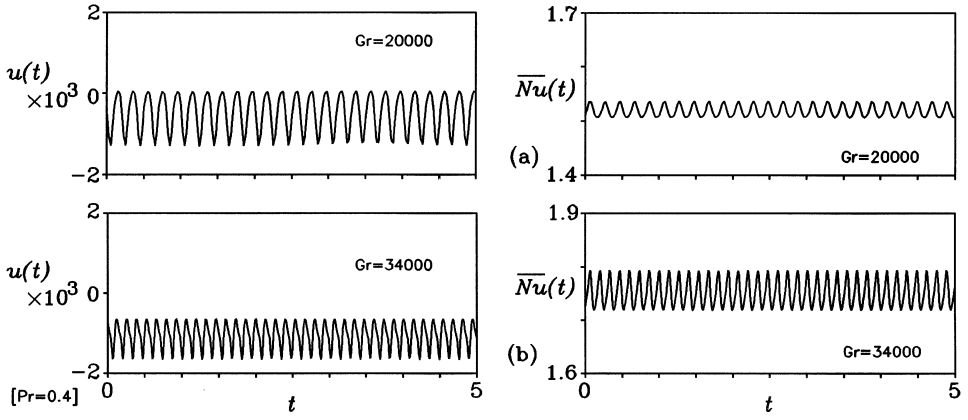

Fig. 10. Time evolutions of $u(t)$ and $\overline{Nu}(t)$ in the solution branch of $N_{(\text{cells on top})} = 4$: (a) $Gr = 2 \times 10^4$; (b) $Gr = 3.4 \times 10^4$.

number when the number of the cells on the top of the annulus is increased (or decreased). And the flow with the more cells on top of the annulus has the greater overall Nusselt number than other flows with fewer cells: $\overline{Nu}_{\text{time}}(4) > \overline{Nu}_{\text{time}}(3) > \overline{Nu}_{\text{time}}(2) > \overline{Nu}_{\text{time}}(1)$, where the numbers in the parentheses represent $N_{(\text{cells on top})}$. Independently of the present investigation for the annular geometry, Le Quéré [27] studied multiple solutions in two-dimensional convection of air in a tall cavity with an aspect ratio of 16, and found multiple solutions characterized by the numbers of cells. For convection in a tall cavity, the mean Nusselt numbers corresponding to the multiple solutions differed very little. In the present configuration, the different number of cells yields large local variations of Nusselt numbers (Fig. 12), and consequently, the difference in overall heat transfer is relatively larger than that of the tall cavity [27]. The result of Fig. 13 was obtained with the $(r \times \phi)$ mesh of (17×257).A test of

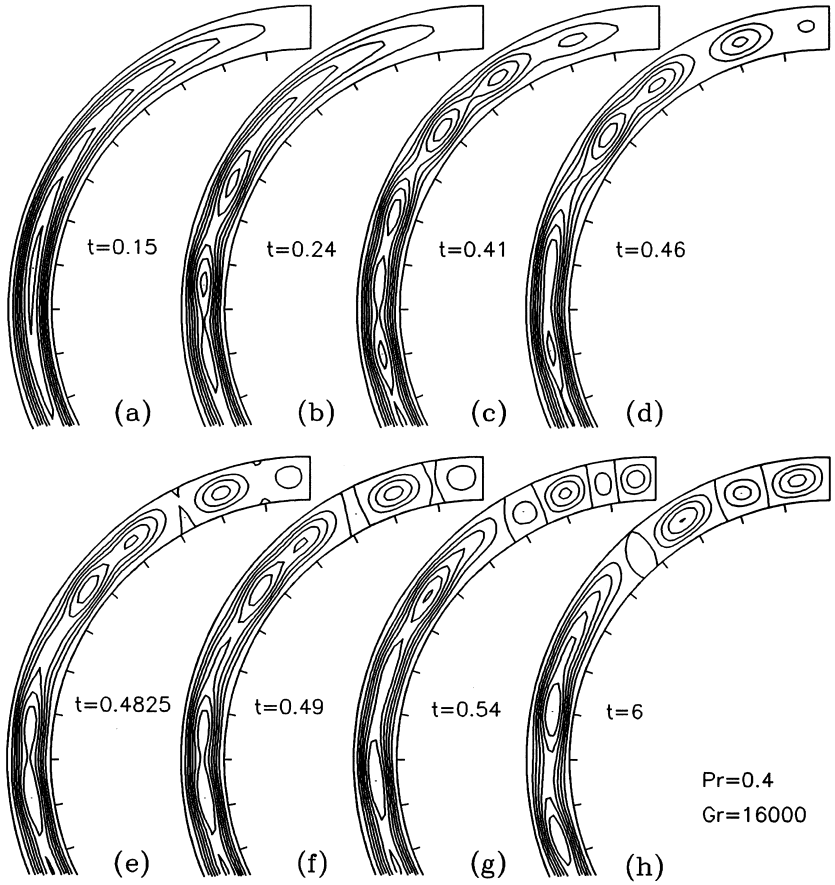

Fig. 11. A transient development of the flow patterns with $Gr = 1.6 \times 10^4$: (a) $t = 0.15$; (b) $t = 0.24$; (c) $t = 0.41$; (d) $t = 0.46$; (e) $t = 0.4825$; (f) $t = 0.49$; (g) $t = 0.54$; (h) $t = 6$. The initial conditions are $\vec{u} = \theta = 0$, and the inner cylinder is suddenly heated to $\theta = 1$.

grid-dependency was made for $Gr = 10^4$ and 3×10^4; when using (25×257), the difference in $\overline{Nu}_{\text{time}}$ was less than 1%.

For the flows at $Gr \leqslant 4.5 \times 10^4$, it has been observed that the shape and strength of the two, three and four cells on the top of the annulus remain almost unvarying during the oscillation period (Figs 5–7, and 9). The angles representing the location of separation points between the cells on the inner cylinder (Fig. 2) are plotted in Fig. 14 as functions of Gr. The approximate shape of cells on the top can be seen from the figure. In the flows with $N_{(\text{cells on top})} = 2$, the cell on the uppermost part of the cylinder grows in size (ϕ_1), with increase of Gr. When the flow has $N_{(\text{cells on top})} = 3$, the size of the mid cells ($\phi_2 - \phi_1$) becomes large, as Gr is increased. For the flows with $N_{(\text{cells on top})} = 2$ and 3, the region occupied by the cells on the top also becomes wide, but approaches a finite limit, as Gr is increased: ϕ_2 and ϕ_3 for $N_{(\text{cells on top})} = 2$ and 3, respectively. When the flow has $N_{(\text{cells on top})} = 4$, however, the size of the cells is nearly unvaried.

As mentioned above, the shape and the strength of the cells on the top of the annulus remain almost unvarying during the oscillation period, when Gr is relatively small ($Gr \leqslant 4.5 \times 10^4$). However, the cells also undergo oscillatory motion in the shape and the strength, and new transition phenomena of flow patterns occur at high Gr. The branches of solutions at $Gr \geqslant 4 \times 10^4$ are presented in Fig. 15. The observed phenomena (up to $Gr = 8 \times 10^4$) are as follows:

(1) $N_{(\text{cells on top})} = 2$: The two-cell pattern is maintained.
(2) $N_{(\text{cells on top})} = 3$:
   (i) At $Gr \leqslant 4.8 \times 10^4$, the three-cell pattern is maintained.
   (ii) At $5 \times 10^4 \leqslant Gr \leqslant 5.4 \times 10^4$, the third cell interfaced with the chain of like-rotating cells in the vertical section is contracting and expanding in size, during the oscillation period.
   (iii) For $Gr \geqslant 5.6 \times 10^4$, the third cell appears and disappears periodically.
(3) $N_{(\text{cells on top})} = 4$:

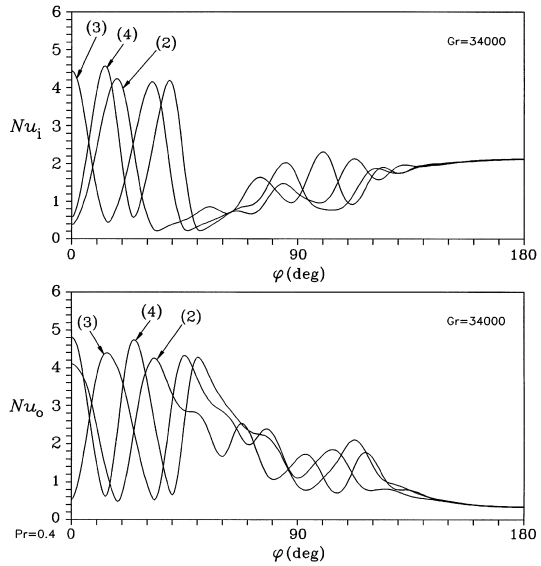

Fig. 12. Instantaneous local Nusselt numbers along the inner (Nu_i) and outer (Nu_o) cylinders at the time when the overall Nusselt $\overline{Nu}(t)$ has its time-averaged value, for the solution branches of $N_{(\text{cells on top})} = 2$, 3, and 4 with $Gr = 3.4 \times 10^4$. The numbers in the parentheses represent $N_{(\text{cells on top})}$.

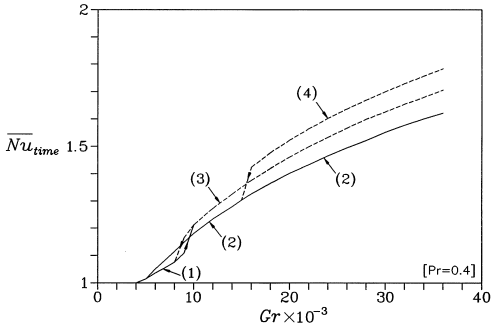

Fig. 13. Time-averaged overall Nusselt number ($\overline{Nu}_{\text{time}}$). In the non-periodic regime of Gr, integration is carried out from $t = t_0$ to $t = t_0 + 15$, and the last part of data for $\overline{Nu}$ are averaged over the time interval of $\Delta t = 10$. The numbers in the parentheses represent the branches of the solutions, $N_{(\text{cells on top})}$.

(i) At $Gr \leqslant 4.6 \times 10^4$, the four-cell pattern is maintained.

(ii) For $4.8 \times 10^4 \leqslant Gr \leqslant 5.6 \times 10^4$, the fourth cell interfaced with the chain of like-rotating cells is contracting and expanding in size.

(iii) At $Gr \geqslant 5.8 \times 10^4$, two cell-pattern flow occurs, i.e., a transition from the branch of $N_{(\text{cells on top})} = 4$ to that of $N_{(\text{cells on top})} = 2$ occurs near $Gr = 5.8 \times 10^4$. However, the transition from $N_{(\text{cells on top})} = 2$ to $N_{(\text{cells on top})} = 4$ does not occur (Figs 3 and 15).

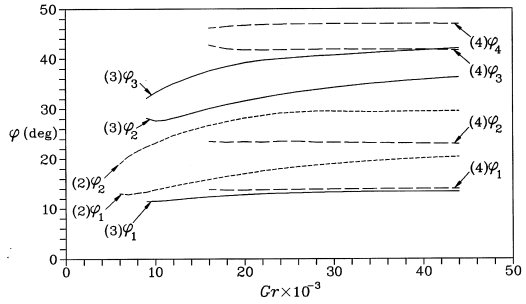

Fig. 14. Angles locating the separation points between the cells on the inner cylinder. The numbers in the parentheses represent $N_{(\text{cells on top})}$. The definition of ϕ_1, ϕ_2, ϕ_3, and ϕ_4 is presented in Fig. 2.

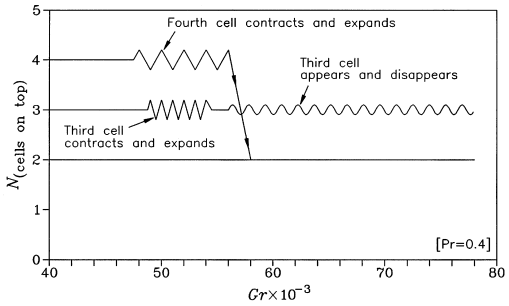

Fig. 15. Diagram showing the solution branches and motion of cells on the top, at high Gr. The cell interfaced with the upper portion of the chain of like-rotating cells in the vertical section of the annulus is represented by the third and fourth cell for the branches of $N_{(\text{cells on top})} = 3$ and 4, respectively.

An example of the flow at high Gr is presented in Fig. 16 with $Gr = 6 \times 10^4$, which shows the periodic appearance of the third cell on the upper part of the annulus. It is to be noted that the vertical section of the annulus in Fig. 16 shows nearly unicellular flow structure, whereas the flows at relatively small Grashof numbers of $Gr = 1.1 \times 10^4$, 1.3×10^4 and 3.4×10^4 in Figs 5–7 display clearly visible two or more like-rotating cells. On the other hand, the streamlines of $Gr = 9000$ in Fig. 2(b) show a single cell in the vertical section. From Figs 2(b), 5–7 and 16, we can see that transitions from unicellular to multicellular, and then from multicellular to approximately unicellular flow occur in the vertical section of the annulus, as Gr is increased. This phenomenon is similar to that of the return to monocellular flow structure observed in the convection in a vertical annulus [17] and a tall cavity [27].

In this study, we have investigated two-dimensional natural convection for a narrow-gap annulus with

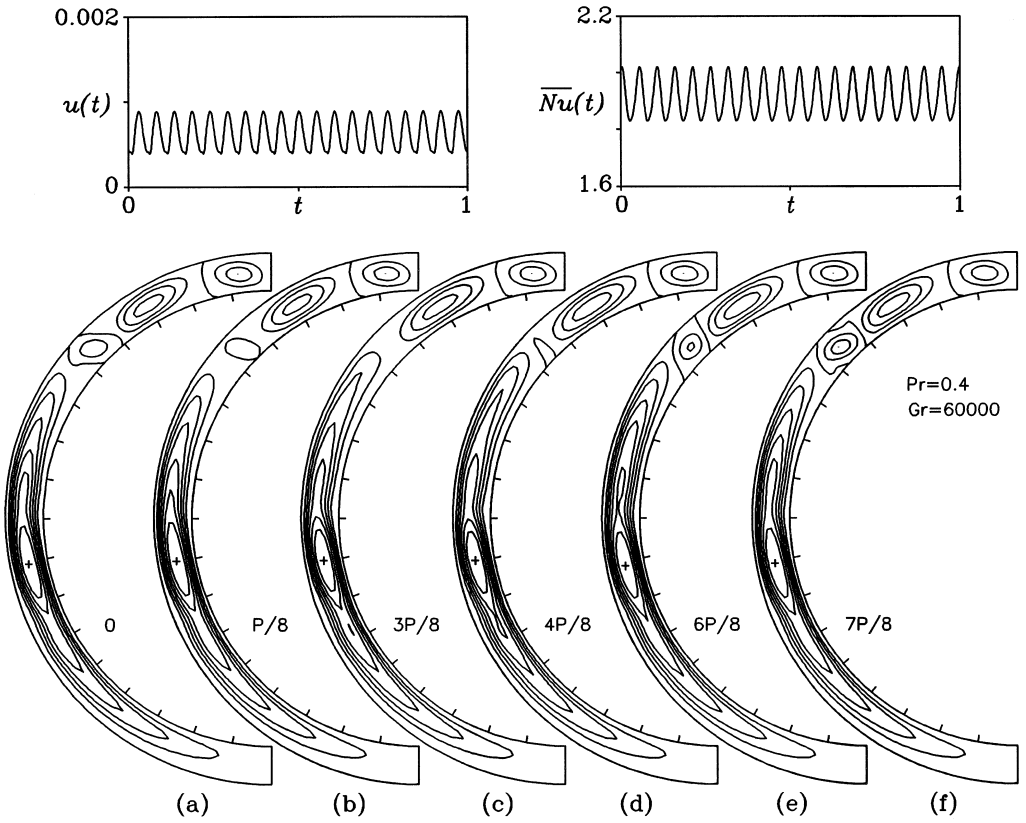

Fig. 16. Plots of $u(t)$, $\overline{Nu}(t)$, and time sequence of streamfunction field over one period of oscillation at $Gr = 6\times10^4$, in the solution branch of $N_{(\text{cells on top})} = 3$ in Fig. 15: (a) at $t = t_1$ at which $u(t)$ takes its minimum value; (b) at $t = t_1 + P/8$; (c) at $t = t_1 + 3P/8$; (d) at $t = t_1 + 4P/8$; (e) at $t = t_1 + 6P/8$; (f) at $t = t_1 + 7P/8$. The cross near $\phi = 100^\circ$ indicates the center of the cell in the vertical section.

$D_i/L = 12$. Powe et al. [4] conducted experimental investigations to classify flow patterns of air, and reported that two-dimensional multicellular flows occurred in the annuli with $D_i/L > 8.5$. The three-dimensional natural convection phenomenon in a narrow horizontal annulus has never been reported in any of the numerical and/or experimental studies. The assumption of two-dimensional flow used in this study is thought to be valid for the convection in a narrow annulus with $D_i/L = 12$ at $Gr \leqslant 8\times10^4$. However, we do not preclude the possibility of three-dimensional flow at sufficient high Gr, and the problem is still waiting for interested readers to study.

4. Conclusions

Natural convection in a narrow horizontal concentric annulus with $D_i/L = 12$ is numerically investigated for a fluid of $Pr = 0.4$. At the intermediate value of $Pr = 0.4$, the combined effect of thermal and hydrodynamic instability yields very complex multicellular flow patterns and interesting transition phenomena. The flows are classified by the number of cells on the top of the annulus, and four branches of solutions are found after the onset of instability of conduction regime. This study found five kinds of multiple solutions characterized by the temporal behavior and spatial structure of flows: (i) dual steady flows; (ii) one steady and one oscillatory flows; (iii) one steady and two oscillatory flows; (iv) dual oscillatory flows; (v) triple oscillatory flows. At small Gr, the like-rotating cells created in the upper part of the annulus drift downward and disappear in the lower region of the annulus. At relatively high Gr, however, the cells do not drift into the lower half of the annulus, and the phenomena of coalescence and separation of two like-rotating cells occur in the lower or upper region of the annulus. As Gr increases, the transition of flow structure shows gradual increase in the number of cells. When Gr is fur-

ther increased, the flow in the vertical section of the annulus reverts to a nearly monocellular structure. The temporal behavior of the flow field is closely related to the motion of cells. As a result, a transition phenomenon of 'steady → oscillatory → steady → oscillatory flow' is found, with increase of Gr. And a transition from a temporally non-periodic flow to a time-periodic flow is also observed.

References

[1] B. Gebhart, Y. Jaluria, R.L. Mahajan, B. Sammakia, Buoyancy-induced Flows and Transport. Hemisphere Publishing Corporation, 1988, pp. 764–771.

[2] J.-S. Yoo, Mixed convection of air between two horizontal concentric cylinders with a cooled rotating outer cylinder. International Journal of Heat and Mass Transfer 41 (1998) 293–302.

[3] J.-S. Yoo, Natural convection in a narrow horizontal cylindrical annulus: $Pr \leqslant 0.3$. International Journal of Heat and Mass Transfer 41 (1998) 3055–3073.

[4] R.E. Powe, C.T. Carley, E.H. Bishop, Free convective flow patterns in cylindrical annuli. Journal of Heat Transfer 91 (1969) 310–314.

[5] R.E. Powe, C.T. Carley, S.L. Carruth, A numerical solution for natural convection in cylindrical annuli. Journal of Heat Transfer 93 (1971) 210–220.

[6] Y.F. Rao, Y. Miki, K. Fukuda, Y. Takata, S. Hasegawa, Flow patterns of natural convection in horizontal cylindrical annuli. International Journal of Heat and Mass Transfer 28 (1985) 705–714.

[7] L.R. Mack, E.H. Bishop, Natural convection between horizontal concentric cylinders for low Rayleigh numbers. Quarterly Journal of Mechanics and Applied Mathematics 21 (1968) 223–241.

[8] J.R. Custer, E.J. Shaughnessy, Thermoconvective motion of low Prandtl number fluids within a horizontal cylindrical annulus. Journal of Heat Transfer 99 (1977) 596–602.

[9] M.C. Charrier-Mojtabi, A. Mojtabi, J.P. Caltagirone, Numerical solution of a flow due to natural convection in horizontal cylindrical annulus. Journal of Heat Transfer 101 (1979) 171–173.

[10] D.B. Fant, J. Prusa, A.P. Rothmayer, Unsteady multicellular natural convection in a narrow horizontal cylindrical annulus. Journal of Heat Transfer 112 (1990) 379–387.

[11] J.-S. Yoo, J.Y. Choi, M.-U. Kim, Multicellular natural convection of a low Prandtl number fluid between horizontal concentric cylinders. Numerical Heat Transfer, Part A 25 (1994) 103–115.

[12] S.A. Korpela, D. Gozum, C.B. Baxi, On the stability of the conduction regime of natural convection in a vertical slot. International Journal of Heat and Mass Transfer 16 (1973) 1683–1690.

[13] S.A. Korpela, A study on the effect of Prandtl number on the stability of the conduction regime of natural convection in an inclined slot. International Journal of Heat and Mass Transfer 17 (1974) 215–222.

[14] Y. Lee, S.A. Korpela, Multicellular natural convection in a vertical slot. Journal of Fluid Mechanics 126 (1983) 91–121.

[15] A. Chait, S.A. Korpela, The secondary flow and its stability for natural convection in a tall vertical enclosure. Journal of Fluid Mechanics 200 (1989) 189–216.

[16] I.G. Choi, S.A. Korpela, Stability of the conduction regime of natural convection in a tall vertical annulus. Journal of Fluid Mechanics 99 (1980) 725–738.

[17] P. Le Quéré, J. Pécheux, Numerical simulations of multiple flow transitions in axisymmetric annulus convection. Journal of Fluid Mechanics 206 (1989) 517–544.

[18] F.H. Busse, Transition to turbulence in Rayleigh–Bénard convection, in: H.L. Swinney, J.P. Gollub (Eds.), Topics in Applied Physics, Vol. 45, Springer–Verlag, 1981, pp. 97–137.

[19] J.-S. Yoo, Dual steady solutions in natural convection between horizontal concentric cylinders. International Journal of Heat and Fluid Flow 17 (1996) 587–593.

[20] T.B. Benjamin, T. Mullin, Notes on the multiplicity of flows in the Taylor experiment. Journal of Fluid Mechanics 121 (1982) 219–230.

[21] S.C.R. Dennis, M. Ng, Dual solutions for steady laminar flow through a curved tube. Quarterly Journal of Mechanics and Applied Mathematics 35 (1982) 305–324.

[22] K. Nandakumar, J.H. Masliyah, H.S. Law, Bifurcation in steady laminar mixed convection flow in horizontal ducts. Journal of Fluid Mechanics 152 (1985) 145–161.

[23] P.J. Zandbergen, D. Dijkstra, Von-Kármán swirling flows. Annual Review of Fluid Mechanics 19 (1987) 465–491.

[24] J.-S Yoo, M.-U. Kim, Two-dimensional convection in a horizontal fluid layer with spatially periodic boundary temperatures. Fluid Dynamics Research 7 (1991) 181–200.

[25] P.J. Roache, Computational Fluid Dynamics. Hermosa, 1972, pp. 53–64.

[26] B.L. Buzbee, G.H. Golub, C.W. Nielson, On direct methods for solving Poisson's equations. SIAM Journal on Numerical Analysis 7 (1970) 627–656.

[27] P. Le Quéré, A note on multiple and unsteady solutions in two-dimensional convection in a tall cavity. Journal of Heat Transfer 112 (1990) 965–974.